Article

A Mathematical Description of the Bone Marrow Dynamics of CAR T-Cell Therapy in B-cell Childhood Acute Lymphoblastic Leukemia

Álvaro Martínez-Rubio [1,2,] *, **Salvador Chulián** [1,2,] , **Cristina Blázquez Goñi** [2,5,] , **Manuel Ramírez Orellana** [6,] ,
Antonio Pérez-Martínez [7,8,] , **Alfonso Navarro-Zapata** [7,] , **Cristina Ferreras** [7,] ,**Victor M. Pérez-García** [3,4,] and
María Rosa [1,2,]

1   Department of Mathematics, Universidad de Cádiz, Puerto Real, Cádiz, Spain
2   Biomedical Research and Innovation Institute of Cádiz (INiBICA), Hospital Universitario Puerta del Mar, Cádiz, Spain
3   Mathematical Oncology Laboratory (MOLAB), Instituto de Matemática Aplicada a la Ciencia y la Ingeniería, Universidad de Castilla-La Mancha, Ciudad Real, Spain
4   Departamento de Matemáticas, Escuela Técnica Superior de Ingenieros Industriales, Universidad de Castilla-La Mancha, Ciudad Real, Spain
5   Department of Pediatric Hematology and Oncology, Hospital de Jerez Cádiz, Spain
6   Department of Paediatric Haematology and Oncology, Hospital Infantil Universitario Niño Jesús, Instituto Investigación Sanitaria La Princesa, Madrid, Spain
7   Translational Research in Pediatric Oncology, Hematopoietic Transplantation and Cell Therapy, IdiPAZ, Hospital Universitario La Paz, Madrid, Spain
8   Pediatric Hemato-Oncology Department, Hospital Universitario La Paz, Madrid, Spain
*   Correspondence: alvaro.martinezrubio@uca.es

1   **Abstract:** Chimeric Antigen Receptor (CAR) T-cell therapy has demonstrated high rates of re-
2   sponse in recurrent B-cell Acute Lymphoblastic Leukemia in children and young adults. Despite
3   this success, a fraction of patients experience relapse after treatment. Relapse is often preceded by
4   recovery of healthy B cells, which suggests loss or dysfunction of CAR T cells in bone marrow. This
5   site is harder to access, and thus is not monitored as frequently as peripheral blood. Understanding
6   the interplay between B cells, leukemic cells and CAR T cells in bone marrow is paramount in
7   ascertaining the causes of lack of response. In this paper, we put forward a mathematical model
8   representing the interaction between constantly renewing B cells, CAR T cells and leukemic cells
9   in the bone marrow. Our model accounts for the maturation dynamics of B cells and incorporates
10   effector and memory CAR T cells. The model provides a plausible description of the dynamics of
11   the various cellular compartments in bone marrow after CAR T infusion. After exploration of the
12   parameter space, we found that the dynamics of CAR T product and disease were independent of
13   the dose injected, initial B-cell load and tumor burden. We also show theoretically the importance
14   of CAR T product attributes in determining therapy outcome, and have studied a variety of
15   possible response scenarios, including second dosage schemes. We conclude by setting out ideas
16   for the refinement of the model.

17   **Keywords:** CAR T, Mathematical Model, Acute Lymphoblastic Leukemia, B cell, Bone Marrow

1. Introduction

19   Chimeric antigen receptor (CAR) T-cell therapy is an immunotherapy technique
20   consisting of the genetic modification of T cells to allow them to recognize specific tumor
21   antigens. The CAR T product is built by obtaining T cells from the patient's blood, and
22   engineering and expanding them in the laboratory. The product is then re-infused into
23   the patient for therapeutic purposes [1]. This is regarded as one of the most promising
24   therapeutic advances in the fight against cancer, and is now integrated into standard

25 care for some hematological malignancies [2,3]. The most successful instance of CAR T
26 therapy is its application to B-cell malignancies, especially when aimed at cells bearing
27 the B-cell common antigen CD19. This marker is widely expressed in B cells, but is absent
28 from other cell types [4], making it an ideal target for immunotherapy. High response
29 rates have been reported in B-cell Acute Lymphoblastic Leukemias and in Diffuse Large
30 B-cell Lymphomas [5–7], leading to the approval of several CAR T products by different
31 regulatory agencies [8,9].

32 This paper focuses on the use of CAR T in B-cell childhood Acute Lymphoblastic
33 Leukemia (ALL). This cancer comprises 80% of pediatric leukemias, which account for
34 25% of all pediatric malignancies [10]. The rate of cure of B-cell ALL has been increasing
35 steadily thanks to improvements in chemotherapy regimes, with around 80% of children
36 achieving complete remission [11]. Prognosis is much worse for patients who experience
37 relapse. This set of patients usually receives additional chemotherapy cycles and possibly
38 hematopoietic progenitor transplants, which are frequently ineffective [12]. It is in this
39 group of highly treated patients that a good rate of response to CAR T therapy has been
40 observed [13]. Clinical trials have shown that CAR T cells are able to expand *in vivo*,
41 eliminate tumor burden and persist in the patient for as long as 2 years [6,14–16].

42 Despite this success, 30 to 50% of patients still experience long term relapse [17].
43 Moreover, 20% of patients fail to achieve remission after CAR T infusion. Some fraction
44 of these relapses are caused by what has been termed "antigenic escape", meaning that
45 tumor cells lose expression of the CD19 antigen and thus avoid the targeted action of CAR
46 T cells. CD19$^+$ relapse, on the other hand, is related to a lack of expansion or persistence
47 of the product [3]. Clinical trials and associated research have found conflicting evidence
48 regarding the relationship between dose, tumor burden and response. It has been
49 pointed out that the reasons for treatment failure may be drug-intrinsic, probably related
50 to characteristics of the patient's T cells before extraction and manufacturing [18,19].

51 CAR T therapy presents a number of treatment-associated toxicities, the most
52 important of which is the so-called cytokine release syndrome (CRS). This condition is
53 related to the fast action of T cells against CD19$^+$ cells, and therefore linked to the level of
54 CAR expansion and tumor burden. Neurotoxicity is another, less elucidated side effect.
55 Finally B-cell aplasia (BCA) is a kind of on-target off-tumor toxicity due to the fact that
56 healthy B cells also express CD19 [20,21]. In fact, BCA in peripheral blood is used as a
57 surrogate marker for CAR T persistence, and loss of BCA is associated with a higher
58 probability of disease recurrence [22,23]. This is because new B cells are continuously
59 being generated in the bone marrow, providing an endless source of stimulation for the
60 CAR T-cell population and acting as an endogenous vaccine [24]. In this regard, it is
61 important to note that most data about the outcome of the therapy, such as absolute
62 leukocyte count, cytokine levels or B cell and CAR T number, come from peripheral
63 blood samples. However, leukemia is a disease of the bone marrow, where blood cells are
64 produced. From that perspective, peripheral blood can be thought of only as a surrogate
65 marker, since what is observed in blood has probably occurred before or is linked to what
66 has previously occurred in bone marrow. Obtaining aspirates or bone marrow biopsies is
67 a more invasive procedure and is not carried out as often as peripheral blood extraction.
68 Thus, data on relevant cellular components in bone marrow dynamics is scarce. Recent
69 studies related to clinical trials have nonetheless recognized the importance of tracking
70 bone-marrow dynamics [24].

71 This is where mathematical modeling comes into play. Mathematical models have
72 long history of application been applied in biology, medicine and oncology. Like animal
73 models, mathematical models offer a simplified representation of a system, providing a
74 tool to explore causal relations and mechanisms. As a recent therapeutic breakthrough,
75 CAR T therapy is starting to lend itself to a mathematical characterization [25]. While
76 there are some studies involving solid tumors [26,27], most focus on hematological
77 malignancies, given the success obtained in this group of cancers. There are general
78 models of leukemia and lymphoma [28–31] and more specific applications in in B-cell

79 lymphoma [32], B-cell chronic lymphoblastic leukemia [33] , T-cell ALL [34], and B-cell
80 ALL [35,36].

81   By integrating mathematical models of B-cell development and T-cell response, the
82 aim is to describe the interaction between cancerous cells, healthy B cells and CAR T cells,
83 with the purpose of reproducing and shedding light on the clinical features typically
84 observed in clinical trials. This can also provide a platform for testing hypotheses related
85 to the success or failure of the therapy and for discussing matters related to the response
86 of T cells to antigen stimulation.

2. Mathematical Model

2.1. Main elements of the model

89   A schematic representation of the compartments and mechanisms accounted for in
90 our mathematical model is shown in Figure 1. There are three main elements. The first
91 is the production of B cells, a sequential process in which cells transit from Pro-B cells
92 (B-cell progenitors that do not yet express the characteristic CD19 surface marker) to
93 immature B cells which exit the bone marrow to complete maturation elsewhere. There
94 are two intermediate steps which are usually called Pre-BI and Pre-BII [37]. This follows
95 the typical compartmentalization of B-cell development [38]. The second element of
96 the model is the leukemic cells. They arise from one of the precursor stages of B-cell
97 development, either Pre-BI or Pre-BII and exit the normal maturation route. They then
98 proliferate with the only restriction of available bone marrow space. Some of these tumor
99 cells can exit the bone marrow and manifest in peripheral blood. Finally, CAR T cells are
100 infused in peripheral blood and then travel to the bone marrow in order to engage with
101 CD19$^+$ cells. They proliferate on encountering them and differentiate into effector cells,
102 inducing the death of antigen-bearing cells and dying shortly afterwards. Part of the
103 expanded population differentiates into long-lived memory cells that retain the ability
104 to proliferate again upon repeated exposure to the antigen [39].

2.2. Hematopoietic and leukemic compartments

106   We described healthy bone marrow by means of compartments $B_i = B_i(t)$, where
107 $i = 0, 1, 2, 3$ represents different stages of maturation of B lymphocytes. B_0 are the B-cell
108 progenitors or Pro-B cells, which do not yet express the B-cell antigen CD19; B_1 are
109 early or Pre-BI cells; B_2 are intermediate or Pre-BII cells; and B_3 are late or immature
110 B cells, ready to enter the blood and complete maturation elsewhere. These three last
111 stages already express the marker CD19. The leukemic clone is given by $L(t)$. The
112 mathematical model for the disease without treatment reads:

$$\frac{dB_0}{dt} = s_B \rho_0 B_0 - \gamma_0 B_0, \tag{1a}$$

$$\frac{dB_1}{dt} = s_B \rho_1 B_1 + \gamma_0 B_0 - \gamma_1 B_1, \tag{1b}$$

$$\frac{dB_2}{dt} = s_B \rho_2 B_2 + \gamma_1 B_1 - \gamma_2 B_2, \tag{1c}$$

$$\frac{dB_3}{dt} = \gamma_2 B_2 - \gamma_3 B_3, \tag{1d}$$

$$\frac{dL}{dt} = s_L \rho_L L \left(1 - \frac{L}{L_{\max}} \right) - \gamma_L L, \tag{1e}$$
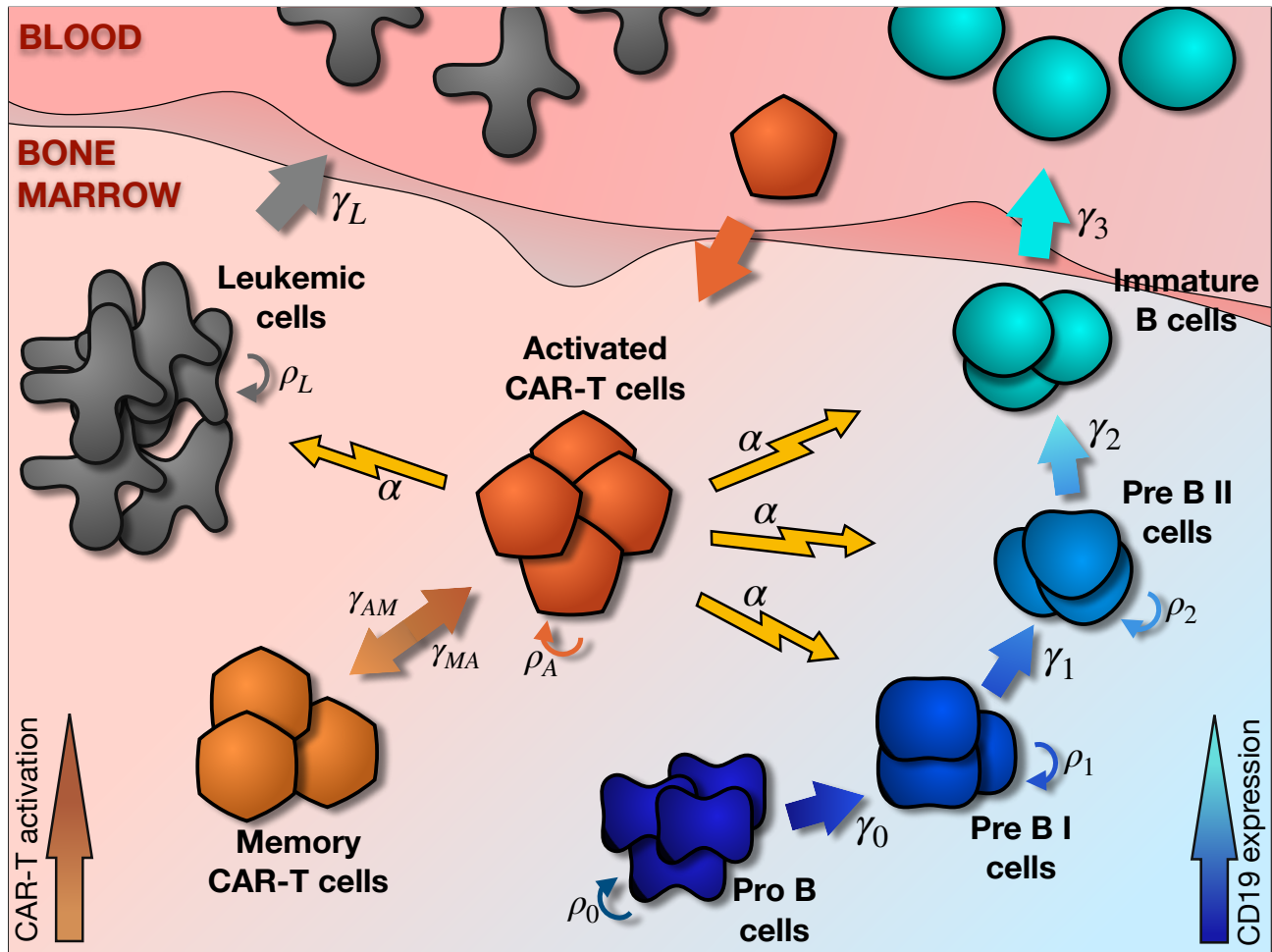
Figure 1. Main biological processes included in the mathematical model. B cells progressively express CD19 as they become more mature. Four maturation stages were considered, namely Pro B, Pre BI, Pre BII and immature B cells. These cell types were assumed to proliferate with rate ρ_i ($i = 1, ..., 4$) and progress with rates γ_i, except for immature B cells which no longer proliferate, leaving bone marrow with an exit rate γ_3. Leukemic cells originate from a B-cell precursor and proliferate with rate ρ_L, invading the bone marrow and eventually migrating to peripheral blood with an exit rate γ_L. CAR T cells are assumed to travel to bone marrow from blood and proliferate with rate ρ_A upon encounters with CD19-expressing cells. They carry out effector functions on CD19 expressing cells with killing capacity α. Pro-B cells are not affected by this action since they do not express CD19. Part of the activated CAR T pool becomes long-lived memory cells with rate γ_{AM}. These cells can regain effector function upon repeated exposure to CD19, with reactivation rate γ_{MA}.

with

$$s_B(t) = \frac{1}{1 + k\left(\sum_{i=0}^{3} B_i + L\right)}, \tag{1f}$$

$$s_L(t) = \frac{1}{1 + k\left(\sum_{i=0}^{3} B_i\right)}. \tag{1g}$$

This paper looks at two main biological processes within each B-cell compartment: proliferation ρ_i and maturation γ_i. It has been previously suggested [40] that the regulation of cell production occurs through a negative feedback signal affecting proliferation $s_B(t)$, where k represents the intensity of the signal. This compartmentalized structure with proliferation, maturation and a regulatory feedback has already been used in mathematical models of B-cell hematopoiesis [41]. In this case, the leukemic clone intervenes in this process by inhibiting the growth of healthy B cells. Leukemic cells, however, can

120 avoid self-inhibition and proliferate (ρ_L) with the restriction of bone marrow space L_{max},
121 invading the bone marrow and leading to a shortage of healthy immune cells [42]. A
122 different signaling function $s_L(t)$ was therefore specified, without the clone. Note that
123 saturation is rarely achieved due to therapeutic action. Finally, we assumed that the
124 invasive character of the clone allows it to exit the bone marrow with rate γ_L and thus
125 be found in blood, which allows it to eventually settle somewhere else [10].

2.3. CAR T-cell compartment

127 Several studies have incorporated CAR T cells in the form of a compartment that
128 expands and acts on B cells and cancer cells [26,32,34–36]. However, clinical evidence
129 suggest that a better description of the dynamics can be achieved by considering two
130 subpopulations [22–24]. This aligns with previous models of immune T-cell response,
131 which considered three compartments for the T-cell populations: naïve, activated or
132 effector, and memory cells [43]. Some models of CAR T response have also included
133 this feature [28,31,33]. The process of T-cell response can be summarized as follows:
134 Naïve T cells enter the system and activate after encountering the corresponding antigen.
135 Activated T cells then undergo fast expansion and carry out effector functions on the
136 antigen-bearing cells. The majority of this expanded pool die shortly after, but part
137 of these cells become memory T cells that can reactivate if they encounter the antigen
138 again in the future. The intricacies of this dual differentiation into effector and memory
139 are not yet fully understood [44,45]. The mathematical representation of de Boer et. al.
140 [46], who fitted data of T-cell response to lymphocytic choriomeningitis virus, has been
141 followed here. This infection induces a persistent immune response and therefore can be
142 helpful in simulating CAR T response. In our case, we assumed naïve cells to come from
143 a single infusion and become activated over a short period of time, thereby omitting
144 the corresponding equation. We denote activated cells by $C_A(t)$, and memory cells by
145 $C_M(t)$. Adding these equations to model (1) yields:

$$\frac{dB_0}{dt} = s_H\rho_0 B_0 - \gamma_0 B_0, \tag{2a}$$

$$\frac{dB_1}{dt} = s_H\rho_1 B_1 + \gamma_0 B_0 - \gamma_1 B_1 - \alpha B_1 C_A, \tag{2b}$$

$$\frac{dB_2}{dt} = s_H\rho_2 B_2 + \gamma_1 B_1 - \gamma_2 B_2 - \alpha B_2 C_A, \tag{2c}$$

$$\frac{dB_3}{dt} = \gamma_2 B_2 - \gamma_3 B_3 - \alpha B_3 C_A, \tag{2d}$$

$$\frac{dL}{dt} = s_L\rho_L L\left(1 - \frac{L}{L_{\max}}\right) - \gamma_L L - \alpha L C_A, \tag{2e}$$

$$\frac{dC_A}{dt} = F(t)(\rho_A C_A + \gamma_{MA} C_M) - \frac{1}{\tau_A}C_A - (1 - F(t))\gamma_{MA} C_A, \tag{2f}$$

$$\frac{dC_M}{dt} = (1 - F(t))\gamma_{AM} C_A - \frac{1}{\tau_M}C_M - F(t)\gamma_{MA} C_M, \tag{2g}$$

with

$$F(t) = \frac{\left(\sum_{i=0}^{3} B_i + L\right)}{h + \left(\sum_{i=0}^{3} B_i + L\right)}. \tag{2h}$$

146 Activated cells $C_A(t)$ proliferate with rate ρ_A and become memory cells $C_M(t)$ with
147 rate γ_{AM}. These processes are modulated by the activation function $F(t)$. This is a
148 continuous function of the level of antigen, and takes values on the interval $[0,1]$. It
149 has been shown previously that a Michaelis-Menten function provides an appropriate
150 functional form [47], saturating for extended antigen exposure. The Michaelis-Menten
151 constant h represents the number of CD19 expressing cells for which activation is half-
152 maximal; we therefore renamed this parameter to activation threshold. This saturating

153 function allowed us to explicitly consider in the model the fact that there is a limit for
154 proliferation during activation, which is not the case in predator-prey models: T-cells
155 commit to a clonal expansion of a given size upon activation of the first parent T-cell
156 [44,48]. Activated cells can also come from memory cells with rate γ_{MA}, a process
157 that again depends on the activation function. When the amount of antigen decreases,
158 proliferation and activation decrease and transition to memory is initiated, thus the term
159 $(1 - F(t))$. With respect to lifetimes, activated cells die with a characteristic time τ_A of
160 the order of days. Memory cells come from activated cells and have a longer lifetime
161 τ_M. They become activated again when the activation function $F(t)$ grows. Finally, the
162 equations for the CD19+ compartments, namely $B_1(t)$, $B_2(t)$, $B_3(t)$ and $L(t)$, include an
163 additional mass action term representing elimination by activated CAR T cells $C_A(t)$,
164 with killing capacity α [49].

165   To sum up, the major assumptions of the model are: (i) the B-cell developmental
166 dynamics specified as a proliferation and maturation process with inhibitory feedback;
167 (ii) the leukemic clone growing without self-inhibition; and (iii) the CAR T population
168 consisting of activated and memory cells controlled by a saturating activation function.

169 *2.4. Parameter estimation*

170   Proliferation and differentiation parameters were taken from Ref. [40], where the
171 evolution of the three CD19+ cellular compartments (B_1, B_2, and B_3) was compared to
172 clinical and literature data to obtain characteristic parameter values. For the additional
173 CD19- compartment B_0, we chose a slower proliferation rate, in accordance with the
174 idea that more immature hematopoietic progenitors cycle at slower rates [50,51]. This
175 compartment also comprises a much smaller subpopulation [38,52], so transition rate
176 was set accordingly. For leukemic cells, assuming a fully invaded bone marrow can
177 exceed its normal homeostatic capacity, we set the saturation value at approximately
178 twice this amount (see [53] for reference values). Leukemic blasts can also be detected in
179 blood. These cells do not follow the usual pathways involved in B-cell generation and
180 release to the bloodstream, so we assumed an exit rate of 0.1%, the exit rate of healthy
181 B cells. As stated before, proliferation rate can be set to either ρ_1 or ρ_2, depending on
182 which B-cell stage we consider as the cell of origin. For simplicity, $\rho_L = \rho_1$ was taken in
183 this paper.

Table 1: Parameter values for the biomathematical model given by Eqs. (2).

Parameter	Meaning	Value	Units	Source
ρ_0	Pro-B proliferation rate	$\ln(2)/8$	day^{-1}	Estimated
ρ_1	Pre-BI proliferation rate	$\ln(2)/1$	day^{-1}	[40]
ρ_2	Pre-BII proliferation rate	$\ln(2)/1.5$	day^{-1}	[40]
γ_0	Transition rate: Pro-B to Pre-BI	0.02	day^{-1}	Estimated
γ_1	Transition rate: Pre-BI to Pre-BII	0.168	day^{-1}	[40]
γ_2	Transition rate: Pre-BII to Immature	0.144	day^{-1}	[40]
γ_3	Blood exit rate	0.288	day^{-1}	[40]
k	Signal intensity	10^{-10}	cell^{-1}	[40]
ρ_{L_n}	Leukemic cell proliferation rate	ρ_1	day^{-1}	Estimated
L_{max}	Leukemic cell carrying capacity	10^{12}	cell	Estimated from [53]
γ_L	Leukemic cell blood exit rate	$0.001 \cdot \gamma_3$	day^{-1}	Estimated
α	Activated CAR T killing capacity	$3 \cdot 10^{-9} - 3 \cdot 10^{-11}$	day$^{-1} \cdot$ cell^{-1}	Estimated from [36]
ρ_C	Activated CAR T proliferation rate	0.9	day^{-1}	[24]
τ_A	Activated CAR T mean lifetime	6.5	day	[24]
α_{AM}	Activated to memory transition rate	0.001	day	[24]
α_{MA}	Memory to activated transition rate	0.33	day	Estimated
τ_M	Memory CAR T mean lifetime	300	day	[24]
h	CAR T activation threshold	$10^8 - 10^{11}$	cell	Estimated

Typical parameter values for the CAR T-cell compartment can be obtained from studies of Tisagenlecleucel kinetics, the FDA-approved CAR T product for B-cell ALL [23,24]. There, the authors fitted patient data to a mixed-effects model and provided values for proliferation rate ρ_C, memory transition rate γ_{AM} and both activated and memory characteristic lifetimes τ_A and τ_M. For the activation of memory cells we assumed a characteristic time of 3 days, given the high intensity of secondary responses [54]. Finally, the activation threshold h depends on the characteristics of the CAR T product, as well as the CAR T killing capacity α. We explored ranges of values that led to realistic scenarios, as we will discuss in the next section. All parameter values and their meanings are listed in Table 1.

To simulate Eqs. (2) we also had to set the initial conditions for the different compartments. For B cells, we started from the homeostatic concentrations that can be obtained by simulating only Eqs. (1a)-(1d). Alternatively, these proportions can be found in Ref. [40]. The total B-cell population in these conditions would be around $3 \cdot 10^{10}$ cells. In the common conditions of cytopenia and after the necessary lymphodepleting chemotherapy, that population should be substantially smaller. We select as the initial state a 1% of that amount leading to a B-cell population of around $3 \cdot 10^8$ cells. With respect to the leukemic clone, clinical trials of CAR T therapy in B-cell ALL report tumor burden ranging from less than 1% to almost 100% of bone marrow mononucleated cells [15,16]. We therefore selected an initial tumor burden in the range $10^{10} - 10^{12}$. Finally, CAR T dose was carefully selected in early clinical trials and lies approximately in the range 0.1 to $5 \cdot 10^6$ cells per kg [6,14–16]. After infusion, CAR T cells in blood decrease sharply due to their distribution to the tissues [22]. We can assume that a substantial part of the product is transferred to the bone marrow, where the majority of CD19 antigen is concentrated. Taking into account pediatric weights we selected the range $10^7 - 10^8$ cells injected.

3. Results

3.1. The mathematical model without B-cell development reproduces clinical data.

Most clinical data obtained in CAR T clinical trials is based on peripheral blood samples. Typical curves for CAR T dynamics can be found in Refs. [22–24]. The usual time course of a successful therapy is as follows: After infusion, CAR T cells are distributed around the body. Next, encounters with tumor or B cells trigger activation and expansion of the CAR T population. After approximately ten days of proliferation, CAR T cells have already expanded by two orders of magnitude or more. Following elimination of the target cells, CAR T-cell numbers undergo a biphasic decline, consisting of an initial fast decay or contraction phase and a slow decay or persistence phase. Peripheral blood, however, lacks the constant production of B cells of the bone marrow, and so we expect the dynamics to be different. Therefore, in order to compare our model with data in blood, the production of B cells during the first post-therapy stages [36] ws neglected, and only Equations (2e)-(2g) were simulated. An example of such simulation is shown in Figure 2.

We observed an initial phase lasting around 10 days of CAR T expansion, during which the leukemic cells still had some time to expand. After the CAR T cells had completed a two-fold expansion, and were mainly composed of effector cells, leukemic cells decreased and eventually disappeared (Figure 2(A)). The CAR T-cell population then contracted rapidly as activated cells died. Memory CAR T cells remained, accounting for the slow decay phase (Figure 2(B)). The magnitude of the expansion and contraction and the characteristic times involved in the response agreed with typical clinical data. This simulation allowed us to confirm the validity of the ranges chosen for the parameter values, specially the killing capacity α and the activation threshold h. In this way we ensured that the results that included B-cell production were reliable.
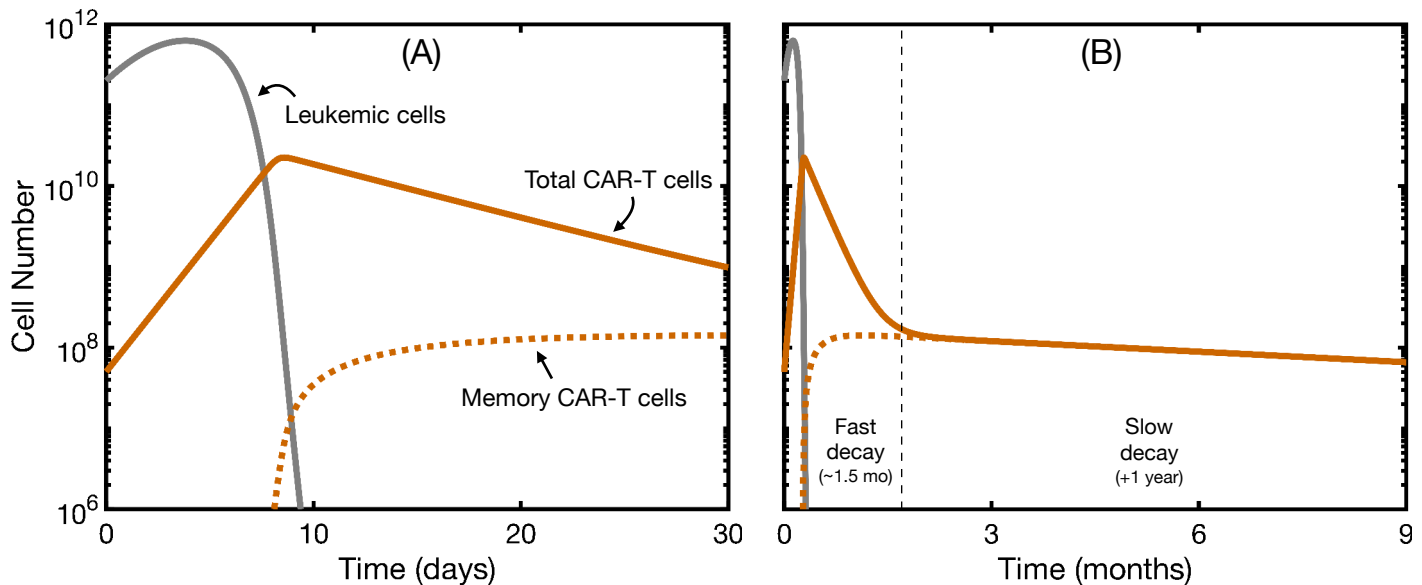
Figure 2. Dynamics of leukemic cells and CAR T cells without new B-cell generation. Simulation of the evolution over time of leukemic cells (solid gray line), total CAR T cells (solid orange line) and memory CAR T cells (dotted orange line). In this simulation we used only Eqs. (2e)-(2g), so we observed no recovery of B cells. The initial state was $L(0) = 2 \times 10^{11}$ cells, $C_A(0) = 5 \times 10^7$ cells and $C_M(0) = 0$ cells. Parameters were as in Table 1 with $\alpha = 3 \times 10^{-10}$ day$^{-1} \cdot$ cell^{-1} and $h = 5 \times 10^8$ cells. **(A)** Dynamics for the first month of therapy. **(B)** Dynamics for the first 9 months of therapy.

3.2. Effector and memory CAR T cells are able to control the disease.

We next analyzed bone marrow expansion scenarios and simulated the model with the complete set of equations. Examples of the results are shown in Figure 3(A). During the first 30 days we observed behavior similar to that of Figure 2(B): Early CAR expansion followed by depletion of all CD19$^+$ cells, healthy and malignant. Pro-B cells increased steadily meanwhile, in response to the shortage of mature B cells. From day 30 onwards, healthy B cells started to recover. Around day 50, CAR T cells responded to this increase: memory cells reactivated and CAR T expanded again. Cycles of CAR T expansion and B-cell reduction ensued, and after 6 months all cell types had reached a steady state and the disease had been controlled. This simulation explains the role of B cells as an endogenous vaccine. Instead of the expected number of activated cells in peripheral blood, we observed their reactivation due to CD19 antigen recovery. The steady although significantly lower level of self-renewing B cells kept CAR T cells in a state of engagement, explaining their persistence.

An interesting prediction coming from this simulation is the change in the distribution of the B-cell population as a result of the therapy. In Figure 3(B) we see the proportion of cells in each subset in homeostatic conditions and the new distribution after therapy. In the latter, B cells were mainly composed of the CD19$^-$ Pro-B cell compartment, and the remaining compartments were ordered according to their maturation stage. In normal conditions the Pre-BII compartment is the most abundant, followed by the immature compartment [38,40]. Reports of successful CAR T therapy in B-cell malignancies indicate B-cell aplasia in peripheral blood as a marker of therapy response [14–16]. While this seems to be in contradiction with the results presented here, where we observe a recovery of B cells, this is actually due to the sensitivity of clinical detection. Indeed, here the immature compartment in the steady state after therapy is composed of approximately 10^6 cells, barely 0.0002% of the total bone marrow capacity. This means the small number of B cells in blood would go undetected. Thus B-cell aplasia in peripheral blood would be compatible with the attempts at B cell recovery in the bone marrow.
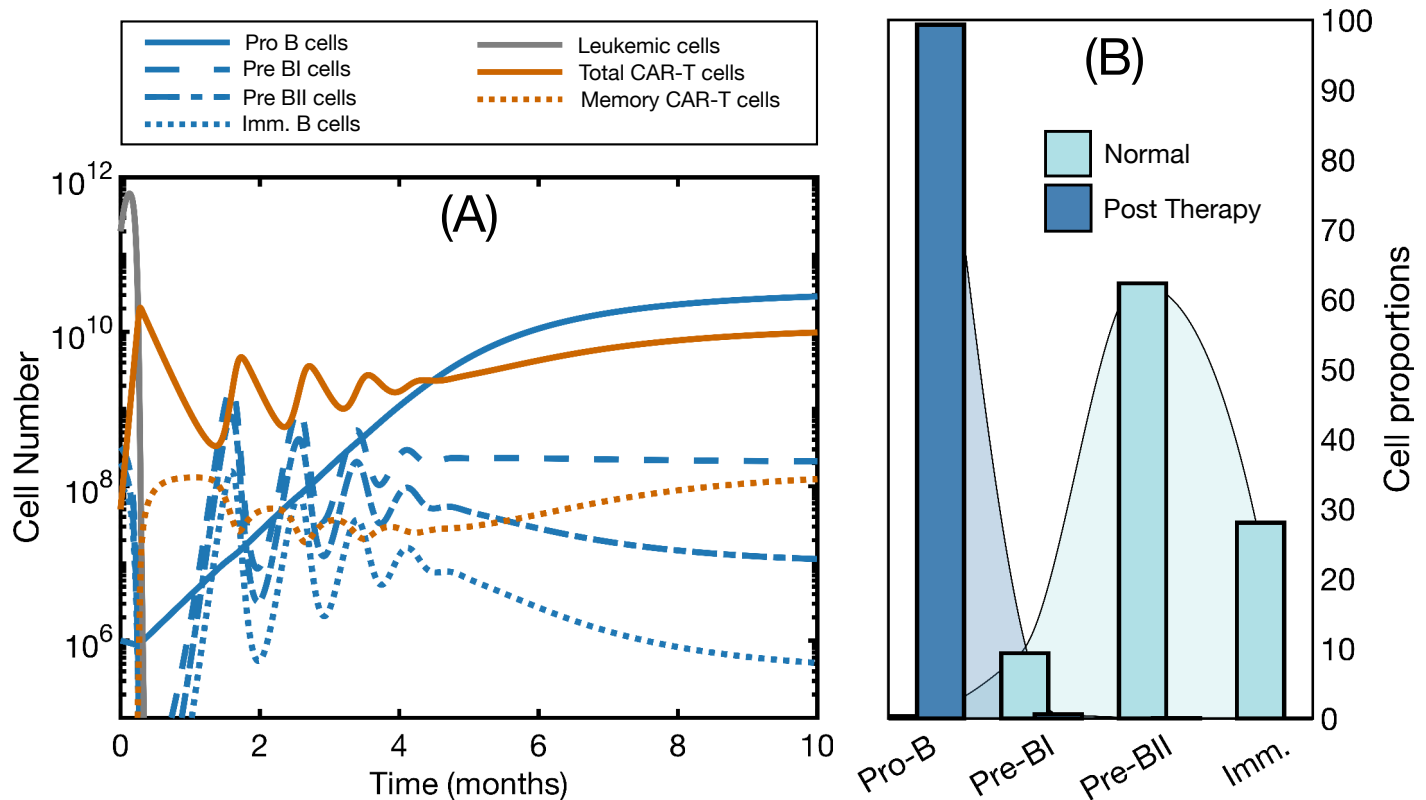
Figure 3. Successful control of the disease in bone marrow. (A) Dynamics of Equations (2). Simulation now includes B cells: Pro-B cells (solid blue line), Pre-BI cells (dashed blue line), Pre-BII cells (dashed-dotted blue line) and Immature B cells (dotted blue line). Initial state is $B_0(0) = 10^6$ cells, $B_1(0) = 3 \times 10^7$ cells, $B_2(0) = 2 \times 10^8$ cells, $B_3(0) = 9 \times 10^7$ cells, $L(0) = 2 \times 10^{11}$ cells, $C_A(0) = 5 \times 10^7$ cells and $C_M(0) = 0$ cells. Parameters are those of Table 1 with $\alpha = 3 \times 10^{-10}$ day^{-1} · cell^{-1} and $h = 10^9$ cells. **(B)** Proportions of B cell subsets in bone marrow, relative to the total B-cell population, under normal conditions (light blue) and after successful CAR T therapy (dark blue). Density plots are a continuous representation of the proportions, obtained by interpolation.

3.3. Initial state does not affect CAR T expansion and outcome

We next studied the effect of the initial state on therapy outcome and CAR T expansion. Clinical trials have investigated the safe dosage regime and the influence of tumor and CD19 burden. In Figure 4 we show the results obtained for different initial values for leukemic cells (A), total B cells (B) and CAR T cells (C). None of these factors had an impact on the expansion and final outcome of the therapy, for a range of parameters justified with clinical information (see parameter estimation). The major effect was a small delay of up to three days in expansion when varying the CAR T dose by an order of magnitude. This agrees with clinical reports returning no dose-exposure relationship [14–16] and no clear influence of tumor burden on CAR T expansion [22–24]. The explanation could lie in the fact that T cells expand *in vivo* in response to stimulation, but in an antigen-independent manner [55,56]. This would also explain why therapy failure seems to be more closely linked to the characteristics of the product rather than to the characteristics of the disease. We will address this point in more detail in the next subsection.

3.4. CAR T product characteristics determine therapy success or failure

We have previously shown an example of disease control (Figure 3). Having noted the limited influence of the initial state on therapy outcome, we turned to CAR T product characteristics to see whether we could explain scenarios of lack of response. As discussed in the introduction, there are two kinds of relapse, CD19⁻ and CD19⁺. In order to simulate the former we would need to describe CD19 expression with a continuous variable or include a CD19⁻ leukemic clone compartment. We therefore restricted the
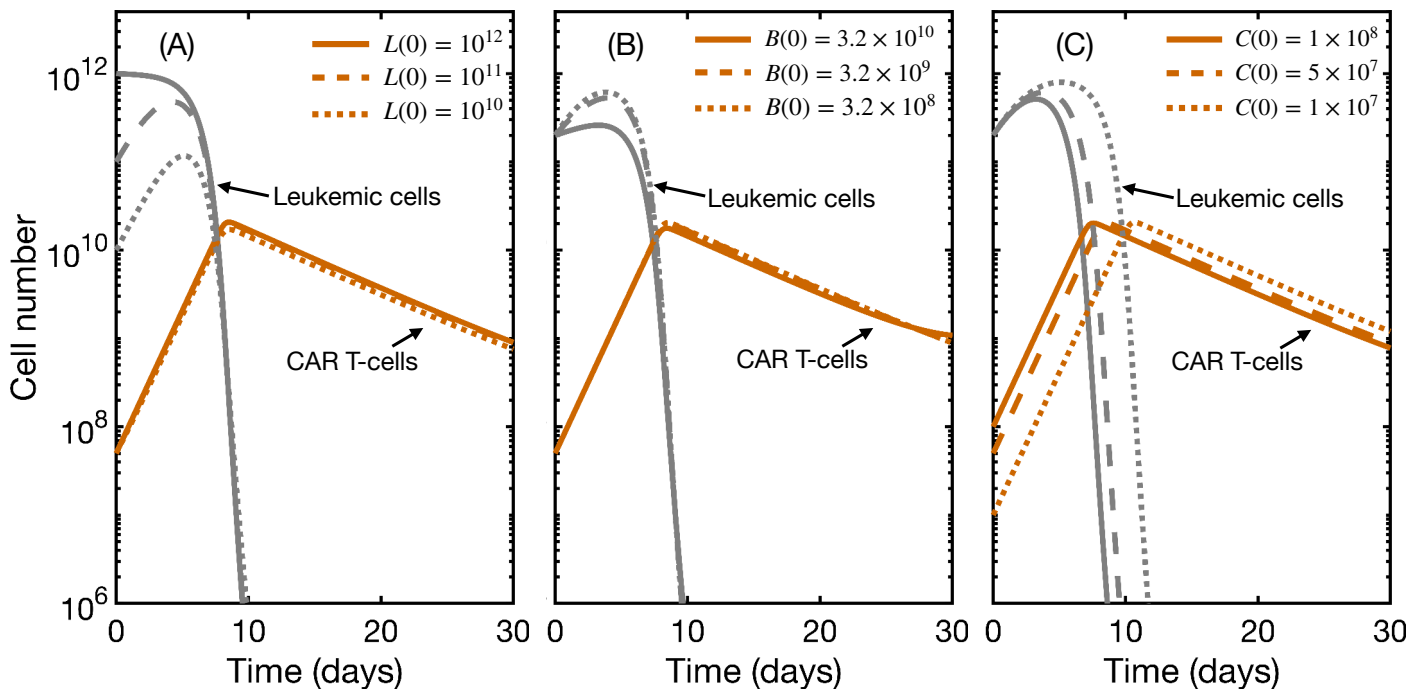
Figure 4. Influence of initial tumor load, B-cell level and CAR T dose on therapy outcome. Evolution with time of leukemic cells (gray) and total CAR T cells (orange) for different initial configurations (In decreasing order: solid, dashed, dotted lines). When unchanged, initial values are $B_0(0) = 10^6$ cells, $B_1(0) = 3 \times 10^7$ cells, $B_2(0) = 2 \times 10^8$ cells, $B_3(0) = 9 \times 10^7$ cells, $L(0) = 2 \times 10^{11}$ cells, $C_A(0) = 5 \times 10^7$ cells and $C_M(0) = 0$ cells. Parameters are those of Table 1 with $\alpha = 3 \times 10^{-10}$ day^{-1} · cell^{-1} and $h = 10^9$ cells. **(A)** Influence of tumor burden. **(B)** Influence of B-cell burden, defined as the sum of all B-cell compartments. **(C)** Influence of CAR T dose.
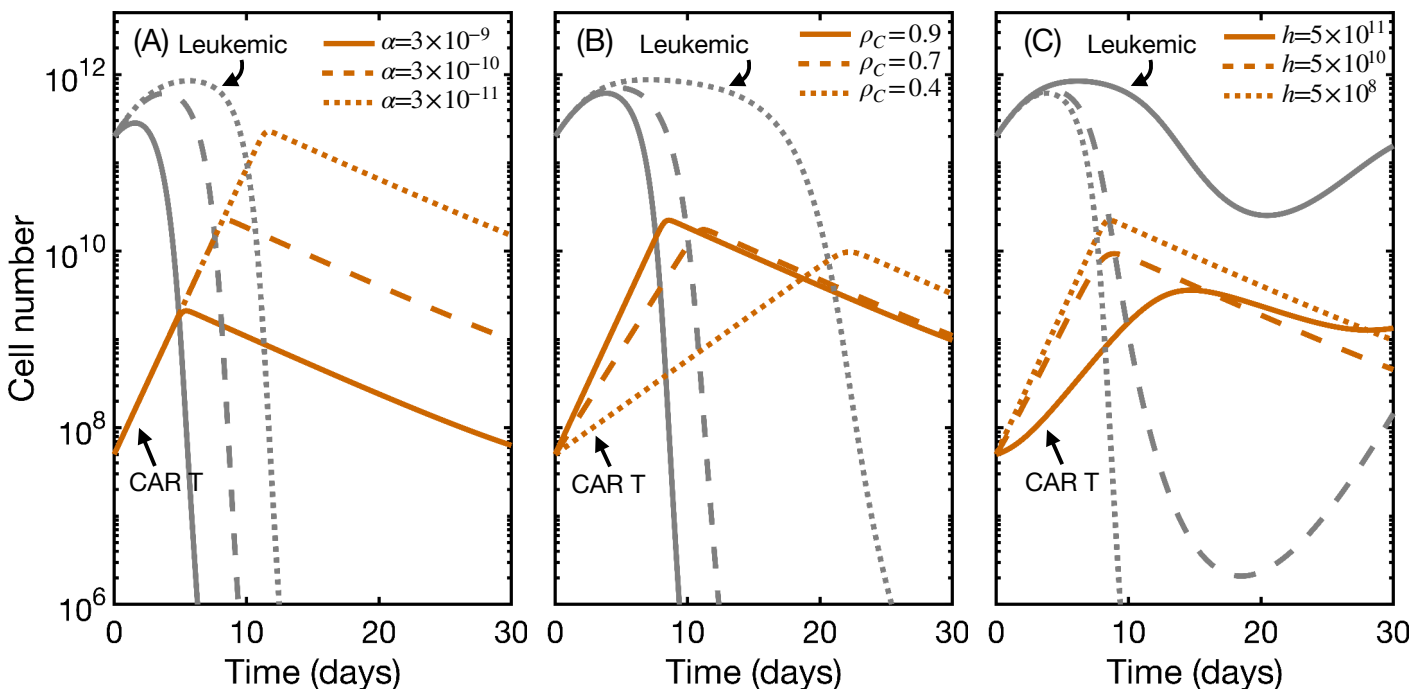
Figure 5. Influence of CAR T product characteristics. Evolution in time of leukemic cells (gray) and total CAR T cells (orange) for different CAR T product attributes (In decreasing order: solid, dashed, dotted lines). Initial state is $B_0(0) = 10^6$ cells, $B_1(0) = 3 \times 10^7$ cells, $B_2(0) = 2 \times 10^8$ cells, $B_3(0) = 9 \times 10^7$ cells, $L(0) = 2 \times 10^{11}$ cells, $C_A(0) = 5 \times 10^7$ cells and $C_M(0) = 0$ cells. The remaining parameter values are those of Table 1 with $\alpha = 3 \times 10^{-10}$ day^{-1} · cell^{-1} and $h = 5 \times 10^8$ cells. **(A)** Influence of tumor-killing capacity. **(B)** Influence of activation threshold. **(C)** Influence of proliferation rate.

analysis to CD19$^+$ relapses. Clinical trials agree that non-responding patients show limited and slower CAR T expansion and shorter persistence, being unable to remove the tumor burden completely [14–16].

In order to reproduce this scenario, we explored the space of parameters delimited by α, the killing capacity of CAR T cells; h, the activation threshold; and ρ_C, the proliferation rate, the three parameters related to CAR T cells and their action. We first simulated the model for different values of one parameter while keeping the other two constant. Results for the first 30 days of treatment are shown in Figure 5. Contrary to what happened with the initial state, here we observed changes in fold expansion and time to peak expansion. Intuitively, shorter proliferation rate (C) and higher activation threshold (B) led to delayed expansion, in some cases being unable to control the malignancy. In fact, products with high activation threshold may lead to therapy failure in cases of low CD19 burden (Figure S1). On the other hand, lower killing capacity implied increased expansion. The explanation is clear in the light of the model equations: when the CAR T cells were unable to eliminate tumor cells, the activation function $F(t)$ remained active and proliferation continued, until there were enough CAR T cells to reduce the tumor burden.

Taking the three results together, we could identify regions of the parameter space related to complete or negative response. In Figure 6(A) we show the number of leukemic cells at day +30 (L_{30}), in logarithmic scale, for pairwise combinations of parameters α, ρ_C and h, while keeping the excluded parameter constant. Each parameter range was discretized into 200 evenly spaced values (linearly spaced for ρ_C and logarithmically spaced for α and h). We note that the killing capacity α was the least important parameter, observing more variation over the ranges of the activation threshold and proliferation rate. As seen in the previous figure, higher proliferation rates and lower activation thresholds were required for complete response. To illustrate the evolution with time of CAR T cells, leukemic cells and B cells in these scenarios, Figure 6(B) gives six examples of the results of the model simulations for the first 6 months of treatment. The three CD19$^+$ B-cell compartments B_1, B_2 and B_3 are plotted together. For each heatmap, we show an example of a responding (R) and a non-responding (NR) patient. Responding patients were defined by the absence of leukemic cells at day 30 ($L_{30} < 1$). Non-responding patients are defined as those with presence of tumor clones on that same day ($L_{30} \geq 1$). The interesting feature of this figure is in analyzing the variety of possible responses. The three responding patients displayed here showed similar behavior, comparable to that of Figure 3: Expansion followed by decay and oscillations. We found that the disease could be controlled for a range of fold expansions. The relative proportion of activated to memory cell was constant, since we were not modifying transition rates γ_{AM} and γ_{MA}. The level of steady state CAR T cells did change and was related to the magnitude of the initial expansion. For the non-responding patients, we observed more variety. First of all, disease recurrence can occur for different magnitudes of expansion, from one to three orders of magnitude (bottom and middle subfigures respectively). Secondly, this recurrence is detectable from the first to the third month after infusion (top and middle subfigures respectively). The level of B cells increased at the time of relapse, which was consistent with the reported association between loss of BCA and likelihood of relapse. Leukemic cells and CAR T cells were also subject to the oscillations that were observed in responding patients, and correspond to cycles of reactivation and decay. Although this model is not reducible to a Lotka-Volterra model, due to the existence of an activation function, these cycles can be interpreted in the same way: an increase in leukemic cells occurred after the decay of activated CAR T cells, which then regrew in response to the recurring clone. Interestingly, in some cases the therapy was able to control the disease after reactivation. This behavior has been observed in simulations of simpler models. In Ref. [36] the authors suggested that this scenario would not be observed in the clinical context due to the prompt actions taken after any signs of disease recurrence. Finally, leukemic cells and CAR T could also coexist in equilibrium (top subfigure).
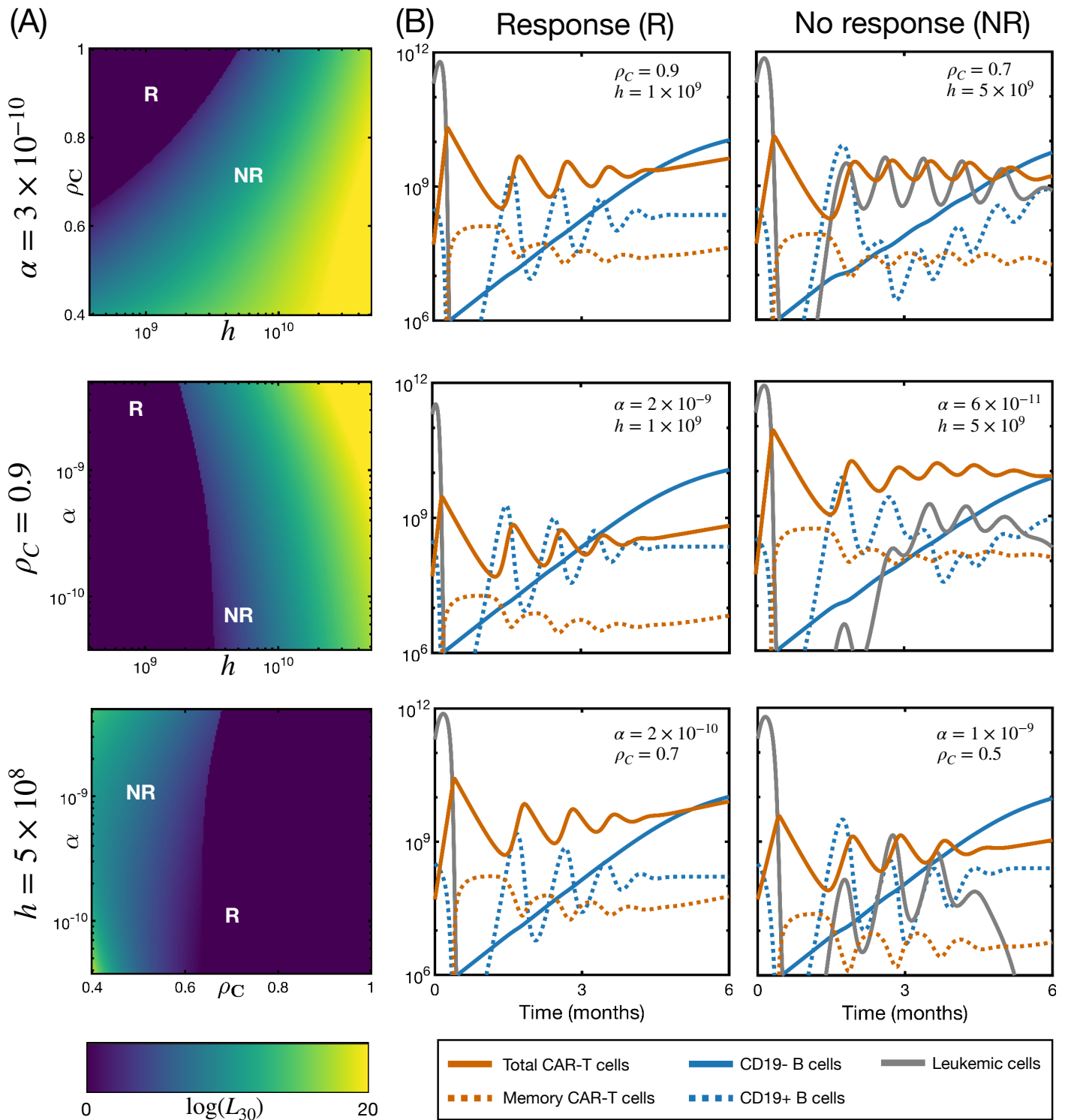
Figure 6. Exploration of parameter ranges for the dynamics of responding (R) and non-responding (NR) patients. (A) Number of leukemic cells at day +30, in logarithmic scale, for different regions of the parameter space. The unchanged product attribute is displayed on the Y-axis. The remaining parameter values are those from Table 1. **(B)** Examples of responding and non-responding patients for the first 6 months of therapy. Parameter values are marked in subfigure (A). Represented are activated and memory CAR T cells (solid and dotted orange line, respectively), leukemic cells (solid gray line) and CD19⁻ and CD19⁺ B cells (solid and dotted blue lines respectively). The initial state of the simulations in this Figure is $B_0(0) = 10^6$ cells, $B_1(0) = 3 \times 10^7$ cells, $B_2(0) = 2 \times 10^8$ cells, $B_3(0) = 9 \times 10^7$ cells, $L(0) = 2 \times 10^{11}$ cells, $C_A(0) = 5 \times 10^7$ cells and $C_M(0) = 0$ cells.
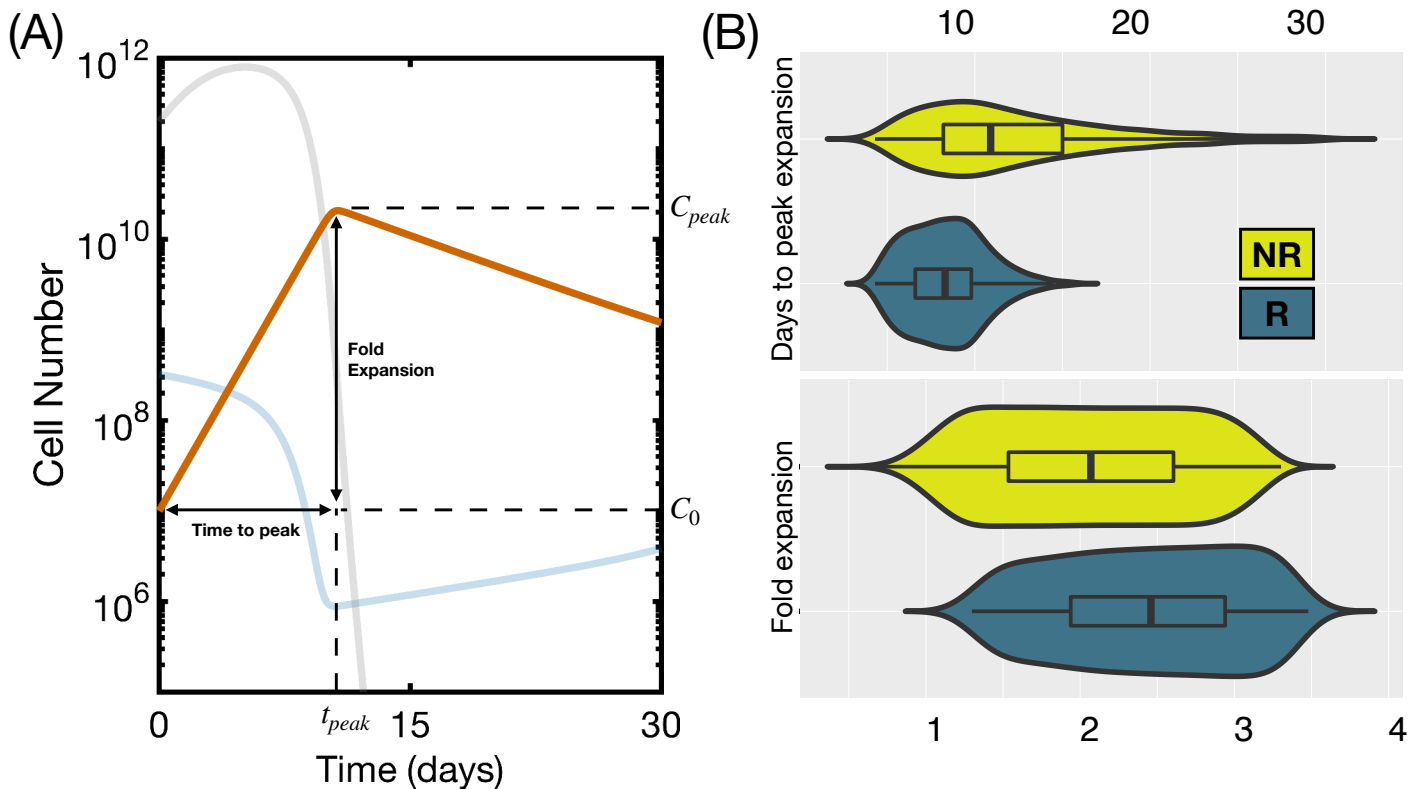
Figure 7. Characteristics of product expansion for Responding (R) and Non-Responding (NR) patients. **(A)** Graphical representation, on a typical simulation, of the characteristics of the product expansion. **(B)** Differences in time to peak and fold expansion for 4000 simulated patients with parameters from Table 1 and α in the range $5 \times 10^{-11} - 5 \times 10^{-9}$ day^{-1} · cell^{-1}, h in the range $5 \times 10^9 - 5 \times 10^{11}$ cells and ρ_C in the range $0.4 - 1$ day^{-1}. Initial state was set to $B_0(0) = 10^6$ cells, $B_1(0) = 3 \times 10^7$ cells, $B_2(0) = 2 \times 10^8$ cells, $B_3(0) = 9 \times 10^7$ cells, $L(0) = 2 \times 10^{11}$ cells, $C_A(0) = 5 \times 10^7$ cells and $C_M(0) = 0$ cells. The boxplot shows median and first and third quartiles.

340   To conclude this exploration, we performed 4000 simulations of the model with
341 the three parameters α, h and ρ_C varying in the ranges specified throughout this section.
342 Specifically, we took 10 evenly spaced values of ρ_C in the interval $0.4 - 1$; 20 logarith-
343 mically spaced values of α in the range $5 \times 10^{-11} - 5 \times 10^{-9}$ and 20 logarithmically
344 spaced values of h in the range $5 \times 10^8 - 5 \times 10^{10}$. We identified responding and non-
345 responding patients as explained above and computed the level of expansion of CAR
346 T cells, defined as $\log(C_{peak}/C_0)$, and the time to peak expansion t_{peak} for each group.
347 Results are shown in Figure 7. This particular range and number of simulations yielded
348 a proportion of responding to non-responding patients of 80 to 20, similar to the early
349 response rate recorded in clinical trials [17]. Non-responding patients took longer to
350 achieve the maximum level of CAR cells and had lower fold expansion (Figure 7(B).
351 $p < 10^{-26}$, Wilcoxon rank-sum test).

352 *3.5. Second infusion in non-responding patients may improve the therapy outcome*

353   A common therapeutic solution for non-responding patients is to reinfuse the origi-
354 nal product, opening the door to the design of dose fractionation schemes. Studies of
355 optimal combinations of timing and dosage are common in chemotherapy and radio-
356 therapy regimes. The main difference here is that CAR T cells expand and operate in
357 relation to the tumor, so standard pharmacokinetic and pharmacodynamic approaches
358 are not applicable.
359   We explored this issue using the mathematical model. For the three non-responding
360 patients in Figure 6, we simulated repeated CAR T cell therapy in three different ways.
361 First, when the tumor reached 10^8 cells, a second dose of 5×10^8 CAR T cells from the

362 original product was reinfused in silico (Figure 8(A)). Secondly, we did the same thing
363 but increasing the number of cells injected in the second dose (Figure 8(B)). Finally,
364 we simulated the infusion of a newly manufactured product with improved attributes
365 (Figure 8(C)), according to the exploration performed in the previous subsection. We
366 observed that a standard re-infusion was not enough to control the relapse. A higher
367 dose could be effective in a subset of patients, while infusing an improved product
368 turned out to be the best option. This agrees with the previous findings that the in-
369 teraction of product and tumor is critical to understand the therapy outcome. Unlike
370 chemotherapeutic drugs, which are typically modeled as a decaying concentration, this
371 therapy expands and contracts depending on the target. These tangled dynamics are
372 responsible for the qualitative differences with a typical dose fractionation scheme, and
373 suggests the need for a deeper investigation of the molecular basis of T-cell and cancer
374 cell interaction. When infusing a different improved CAR, this second product eventu-
375 ally became dominant in the CAR T-cell subpopulation (Figure S2). Clonal dynamics of
376 this kind within the product have already been reported [57], opening the door to an
377 evolutionary exploration of the therapy, another feature that is absent in other types of
378 treatment.

379   To explore the full range of product attributes, we repeated the simulations shown
380 in Figure 6 with the reinfusion protocol. As explained above, a second dose was given
381 when tumor reached 10^8 cells or the highest value below that number. Where there
382 was no initial response, a second dose was infused computationally at day +30. The
383 results showed that the regions associated with success and failure remained invariant,
384 reinforcing the conclusion that a single reinfusion of the original product would not be a
385 successful strategy in general (Figure S3).

4. Discussion

387   CAR T-cell therapy is the most promising therapeutic option for recurrent B-cell
388 acute lymphoblastic leukemia in children. The recent approval of the first drug by the
389 US and EU drug administrations has culminated three decades of research in adoptive
390 transfer of autologous, genetically modified T cells. Clinical trials have shown good
391 rates of response and long-term remission. After four generations, the CAR T construct
392 has achieved enough expansion and persistence potential to induce successful responses.
393 The persistence of CAR T cells in the organism, acting as a surveillance mechanism, is
394 thought to be promoted by the continuous generation of B cells in bone marrow, acting
395 as an endogenous vaccine [24]. The interaction between renewing B cells, CAR T cells
396 and leukemic cells in the bone marrow is therefore likely to predict the outcome of the
397 therapy. The lack of extensive bone marrow data due to the more invasive way it must
398 be extracted means that other means of studying these dynamics must be explored.

399   In this study, we aimed to incorporate into mathematical models two elements
400 that have been reported to be important by clinical research. The first was the role of
401 bone marrow as a source of CAR T-cell ongoing stimulation, due to the production of
402 B cells. The second was the kinetics of the product, which had been characterized by
403 a biphasic decline and explained by the existence of two CAR T subpopulations, one
404 effector, the other memory. This was done by building on previous mathematical models
405 of B cell development and CAR T therapy, which had underlined the importance of B cell
406 production in determining therapy outcome. Contrary to the usual mass action term for
407 the proliferation of the CAR T cells, we followed previous models of T-cell response and
408 included an activation function. In this way we accounted for the antigen-independent
409 features of T-cell response. The result was a mathematical model of seven ordinary
410 differential equations, with many of the parameters already studied or available from
411 clinical data.

412   Our first goal was to reproduce the known kinetics of the product and the clinical
413 observations related to the therapy. By omitting the equations related to B-cell production
414 we were able to recover the characteristic curves reported from clinical trials with the
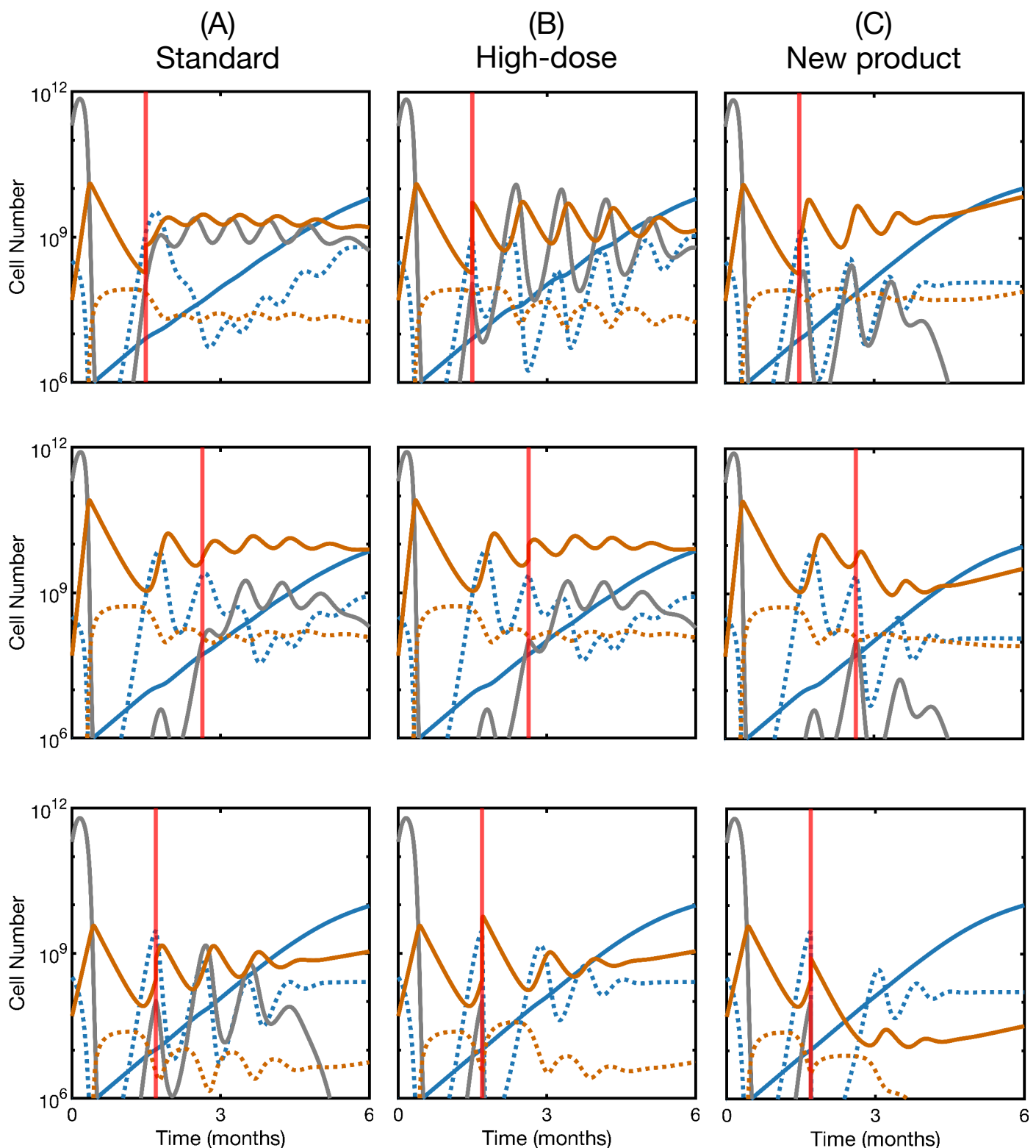
Figure 8. Effect of a second infusion of CAR T cells in non-responding patients. Dynamics of tumor cells, B cells and CAR T cells for the three non-responding patients in Figure 6. **(A)** Standard second dose of 5×10^8 CAR T cells. **(B)** Increased second dose of 5×10^9 CAR T cells. **(C)** Second dose of 5×10^8 CAR T cells of a newly-manufactured product with improved attributes. For the first patient, the new attributes were $h = 5 \times 10^8$ and $\rho_C = 0.9$. For the second patient, the new attributes were $h = 5 \times 10^8$ and $\alpha = 6 \times 10^{-10}$. For the third patient, the new parameters were $\alpha = 5 \times 10^{-8}$ and $\rho_C = 0.7$. We show activated and memory CAR T cells (solid and dotted orange line, respectively), leukemic cells (solid gray line) and CD19⁻ and CD19⁺ B cells (solid and dotted blue lines respectively). The red vertical line represents the time of the second infusion. The initial state for the simulations and the other parameter values were as in Figure 6.

biphasic decline in the number of CAR T cells. We then simulated the production of B cells, describing the differences with the dynamics in peripheral blood. We observed the reactivation of CAR T cells due to the recovery of B cells and the achievement of a steady state which accounted for both the persistence of the drug and the absence of B cells in blood. The model predicted relative proportions of B-cell subsets and CAR T subsets directly attainable from the flow cytometry data of long-term remission patients. In particular, the reorganization of the B-cell subsets, with a predominant CD19⁻ compartment, has recently been reported in patients who respond to anti-CD19 therapy [58]. This otherwise unnoticeable precursor could reach up to 100% of all the B-cell precursors, as shown here. We also noted that peripheral blood and bone marrow dynamics were similar during the first month of therapy, clarifying the relevance of this time scale in assessing response. One of the first clinical trials described recovery of hematogones or normal B-cell progenitors in bone marrow from day 28 onwards, which matches the simulations of our model [15].

Our second goal was to identify which parameters were most relevant in relapse. We first assessed the importance of the initial quantities of B cells, leukemic cells and CAR T cells. None of these factors seemed to influence expansion and outcome. With respect to tumor burden or CD19 burden, clinical trials have reported either no influence or contradictory evidence [22,24,59,60]. There is more agreement about the lack of relationship between dose and response [61]. We then evaluated the influence of CAR T product characteristics, with the hypothesis that some phenotypic properties of the CAR T cells are associated with lack of response [62]. We showed that proliferation rate ρ_C and activation threshold h are relevant in determining response. This seems reasonable, since these are the two factors that have been the subject of improvement in the different generations of CAR T cells. In fact, early generations failed due to impaired activation and expansion [63]. We also showed that a high activation threshold could explain those cases in which low antigen burden is associated with therapy failure [62]. On the other hand, we observed rather counterintuitive behavior when varying the killing capacity α. Lower values of killing capacity meant increased expansion, due to the continuous activation caused by tumor cells that the drug was not able to eliminate. This contradicts the observed fact that non-responding patients have reduced expansion. Nonetheless, when the whole range of parameters was evaluated, we found significant differences in expansion between the groups of responding and non-responding patients. Also, in some cases non-responding patients expand normally. CD19⁺ relapses could then be explained by the impaired effector capacity of the CAR T cells, which can be induced by leukemic cells themselves [64]. Non-responding patients were also shown here to reach maximum expansion later than responding patients, which also agrees with clinical observations. In this case, however, clinical differences were more pronounced [6]. In support of this counterinituitive result, some studies have shown that a product with lower affinity, which here means a lower killing capacity, can yield better results in expansion and persistence [65,66].

We then used the mathematical model to test, in silico, the effectivity of a second dose of CAR T, a procedure that has been carried out in patients that did not respond to the first infusion. We showed that the same product is unlikely to control the disease, while increasing the dose, and especially improving the quality of the product, could be more impactful. Clinical trials have precisely reported little to no success of reinfusions [15,16,67], which could also be related to the lack of lymphodepleting chemotherapy and/or the role of T-regs. A recent study identified the factors associated with complete response after second infusions [68]. These are mainly a higher dose, as reported here, and lymphodepleting chemotherapy before the first dose. Failure of second dose has also been attributed to the development of an immune response against the CAR T [69]. We showed here that it could be due to the dynamical nature of the interaction: The outcome is determined by the parameters that control this interaction, and not by the amounts involved or by their timing, as would happen with chemotherapy. For this

reason, rather than dose-fractioning schemes, the optimal course of action would be to search for ways to affect this interaction. For example, infusions of T-cell specific antigen-presenting cells have been shown to boost anti-tumor response [62,70]. In this line, the model predicts that infusion of B-cells upon relapse could potentially control the disease or delay recurrence in some cases (Figure S4).

A recent review of mathematical models of CAR T-cell therapy [25] suggested a number of requisites that any of these models should include to provide a faithful description of the biological dynamics. The model presented here succeeds in recapitulating antigen-driven expansion, bi-exponential decay and a limited expansion despite large antigen burden. It does so without depending on a piecewise definition of the model, integrating both expansion and decay in the same mathematical framework. The model also allowed for the accommodation of multiple dosages. A point of disagreement was the oscillatory behavior of CAR T cells and B cells. This can be explained analogously to predator-prey dynamics, although the system is not directly reducible to a Lotka-Volterra system of equations. Interestingly, behavior of this kind in bone marrow has been recently reported by a clinical trial [71]. Also, these cycles were predicted to occur in the bone marrow, where B cells are produced, and not in peripheral blood, which is where the kinetics of the product are normally assessed. Given the length and amplitude of the cycles shown here, current protocols of bone-marrow extraction might not be able to detect this phenomenon within the precision of cell abundance determinations.

The model presented here, despite its success in representing a range of clinical observations, is missing some features of non-responding patients. First of all, CD19⁻ relapses demand a different modeling approach, or the inclusion of more compartments, possibly including selection processes. With respect to CD19⁺ relapses, the model was not able to capture long term relapse, occurring from month 3 onwards. We have observed here that, from this date, the system typically reaches a steady state, in coexistence with either healthy B cells (in responding patients) or both leukemic clone and B cells (in non-responding patients). A steady state of this kind is consistent with patients in whom BCA has been ongoing for long periods of time, but not those who either relapse or recover B cells in peripheral blood in the meantime. Also, differences in expansion and time to maximum expansion between responding and non-responding patients should be higher. This may be due to our arbitrary selection of parameter values in their respective ranges, or to the fact that we did not take into account correlations between them. Nonetheless, we cannot discard the possibility that other processes are at work.

Some biological elements may be needed in more exhaustive mathematical models, able to account for more biological phenomena present in CAR T-cell treatments. First, mechanisms of T-cell exhaustion could help in accounting for long term relapses. These mechanisms are thought to be linked to excessive stimulation or activation [72], and are often found in persistent infections such as lymphocytic choriomeningitis (LCM) or cytomegalovirus (CMV) [73]. A mechanism of this kind would attenuate the excessive expansion in patients with lower killing capacity, leading to the death of CAR T cells subjected to continuous stimulation. It should also explain the loss of the CAR T cells in situations of coexistence with the clone, which demands sustained activation and effector functions. Finally, it should also account for the loss of the product after longer periods of coexistence with B cells, which are not as demanding to the CAR T as the clone from the immunological point of view. This would also cause the attenuation of the cycles of expansion and decay.

A second biological element that should be accounted for in mathematical models is a more detailed description of the process of activation, differentiation and renewal of CAR T cells. This part of the system has been shown to be more significant than, for example, the compartmentalization of B-cell development or the initial state. Along these lines, there are studies that explain how the specific subsets of T cells in the initial leukapheresis can be a determinant of the response. For example, central memory T

cells can yield a more effective product than other phenotypes [17]. This suggests that, while a separation in effector and memory T cells is enough to represent the kinetics of the drug, a more detailed description of the subsets could be necessary to explain and interpret therapy outcome.

5. Conclusion

We have presented a mathematical model of CAR T-cell therapy in bone marrow that is able to explain a number of clinical features that have been observed. It can account for the measured kinetics of the drug and for the coincidence of BCA and CAR T persistence. It also agrees in attributing more relevance to product characteristics in determining response. Some of the predictions and properties of the model are easily testable from already existing clinical data, for example by adding panels for B cells and T cells in flow cytometry data. Relative proportions of these cellular subpopulations could help in parameterizing this and other models of CAR T therapy response. The mathematical model also suggests the importance of characterizing the composition of both the infused product and the patient's initial T-cell repertoire. Simple improvements of the mathematical model could explain additional observations, possibly including a more detailed description of the T-cell compartment and the consideration of mechanisms of T-cell exhaustion.

We hope that this study will stimulate mathematical research in this interesting area, in which in-silico modeling can help in finding optimal therapeutic schedules and in suggesting ways for improving treatments with these promising immunotherapies.

Abbreviations

The following abbreviations are used in this manuscript:

CAR	Chimeric Antigen Receptor
ALL	Acute Lymphoblastic Leukemia
CD	Cluster of Differentiation
CRS	Cytokine Release Syndrome
BCA	B-Cell Aplasia
FDA	Federal Drug Administration
LCM	Lymphocytic Choriomeningitis
CMV	Cytomegalovirus

References

1. Levine, B.L.; Miskin, J.; Wonnacott, K.; Keir, C. Global manufacturing of CAR T cell therapy. *Molecular Therapy-Methods & Clinical Development* **2017**, *4*, 92–101.
2. Hartmann, J.; Schüßler-Lenz, M.; Bondanza, A.; Buchholz, C.J. Clinical development of CAR T cells—challenges and opportunities in translating innovative treatment concepts. *EMBO Molecular Medicine* **2017**, *9*, 1183–1197.
3. Brown, C.E.; Mackall, C.L. CAR T cell therapy: inroads to response and resistance. *Nature Reviews Immunology* **2019**, *19*, 73.
4. Sadelain, M. CAR therapy: the CD19 paradigm. *Journal of Clinical Investigation* **2015**, *125*, 3392–3400.
5. Neelapu, S.S.; Locke, F.L.; Bartlett, N.L.; Lekakis, L.J.; Miklos, D.B.; Jacobson, C.A.; Braunschweig, I.; Oluwole, O.O.; Siddiqi, T.; Lin, Y.; others. Axicabtagene ciloleucel CAR T-cell therapy in refractory large B-cell lymphoma. *New England Journal of Medicine* **2017**, *377*, 2531–2544.
6. Maude, S.L.; Laetsch, T.W.; Buechner, J.; Rives, S.; Boyer, M.; Bittencourt, H.; Bader, P.; Verneris, M.R.; Stefanski, H.E.; Myers, G.D.; others. Tisagenlecleucel in children and young adults with B-cell lymphoblastic leukemia. *New England Journal of Medicine* **2018**, *378*, 439–448.
7. Schuster, S.J.; Bishop, M.R.; Tam, C.S.; Waller, E.K.; Borchmann, P.; McGuirk, J.P.; Jäger, U.; Jaglowski, S.; Andreadis, C.; Westin, J.R.; others. Tisagenlecleucel in adult relapsed or refractory diffuse large B-cell lymphoma. *New England Journal of Medicine* **2019**, *380*, 45–56.
8. O'Leary, M.C.; Lu, X.; Huang, Y.; Lin, X.; Mahmood, I.; Przepiorka, D.; Gavin, D.; Lee, S.; Liu, K.; George, B.; others. FDA approval summary: tisagenlecleucel for treatment of patients with relapsed or refractory B-cell precursor acute lymphoblastic leukemia. *Clinical Cancer Research* **2019**, *25*, 1142–1146.
9. Bouchkouj, N.; Kasamon, Y.L.; de Claro, R.A.; George, B.; Lin, X.; Lee, S.; Blumenthal, G.M.; Bryan, W.; McKee, A.E.; Pazdur, R. FDA approval summary: Axicabtagene ciloleucel for relapsed or refractory large B-cell lymphoma. *Clinical Cancer Research* **2019**, *25*, 1702–1708.
10. Wartenberg, D.; Groves, F.D.; Adelman, A.S. Acute lymphoblastic leukemia: epidemiology and etiology. In *Acute Leukemias*; Springer, 2008; pp. 77–93.
11. Pui, C.H.; Yang, J.J.; Hunger, S.P.; Pieters, R.; Schrappe, M.; Biondi, A.; Vora, A.; Baruchel, A.; Silverman, L.B.; Schmiegelow, K.; others. Childhood acute lymphoblastic leukemia: progress through collaboration. *Journal of Clinical Oncology* **2015**, *33*, 2938.
12. Bhojwani, D.; Pui, C.H. Relapsed childhood acute lymphoblastic leukaemia. *Lancet Oncology* **2013**, *14*, e205–e217.
13. Martino, M.; Alati, C.; Canale, F.A.; Musuraca, G.; Martinelli, G.; Cerchione, C. A Review of Clinical Outcomes of CAR T-Cell Therapies for B-Acute Lymphoblastic Leukemia. *International Journal of Molecular Sciences* **2021**, *22*, 2150.
14. Maude, S.L.; Frey, N.; Shaw, P.A.; Aplenc, R.; Barrett, D.M.; Bunin, N.J.; Chew, A.; Gonzalez, V.E.; Zheng, Z.; Lacey, S.F.; others. Chimeric antigen receptor T cells for sustained remissions in leukemia. *New England Journal of Medicine* **2014**, *371*, 1507–1517.
15. Lee, D.W.; Kochenderfer, J.N.; Stetler-Stevenson, M.; Cui, Y.K.; Delbrook, C.; Feldman, S.A.; Fry, T.J.; Orentas, R.; Sabatino, M.; Shah, N.N.; others. T cells expressing CD19 chimeric antigen receptors for acute lymphoblastic leukaemia in children and young adults: a phase 1 dose-escalation trial. *Lancet* **2015**, *385*, 517–528.
16. Gardner, R.A.; Finney, O.; Annesley, C.; Brakke, H.; Summers, C.; Leger, K.; Bleakley, M.; Brown, C.; Mgebroff, S.; Kelly-Spratt, K.S.; others. Intent-to-treat leukemia remission by CD19 CAR T cells of defined formulation and dose in children and young adults. *Blood* **2017**, *129*, 3322–3331.
17. Shah, N.N.; Fry, T.J. Mechanisms of resistance to CAR T cell therapy. *Nature Reviews Clinical Oncology* **2019**, *16*, 372–385.
18. Majzner, R.G.; Mackall, C.L. Clinical lessons learned from the first leg of the CAR T cell journey. *Nature Medicine* **2019**, *25*, 1341–1355.
19. Cheng, J.; Zhao, L.; Zhang, Y.; Qin, Y.; Guang, Y.; Zhang, T.; Liu, C.; Zhou, J. Understanding the mechanisms of resistance to CAR T-cell therapy in malignancies. *Frontiers in Oncology* **2019**, *9*, 1237.
20. Brudno, J.N.; Kochenderfer, J.N. Recent advances in CAR T-cell toxicity: mechanisms, manifestations and management. *Blood Reviews* **2019**, *34*, 45–55.
21. Hirayama, A.V.; Turtle, C.J. Toxicities of CD19 CAR-T cell immunotherapy. *American Journal of Hematology* **2019**, *94*, S42–S49.
22. Mueller, K.T.; Maude, S.L.; Porter, D.L.; Frey, N.; Wood, P.; Han, X.; Waldron, E.; Chakraborty, A.; Awasthi, R.; Levine, B.L.; others. Cellular kinetics of CTL019 in relapsed/refractory B-cell acute lymphoblastic leukemia and chronic lymphocytic leukemia. *Blood* **2017**, *130*, 2317–2325.
23. Mueller, K.T.; Waldron, E.; Grupp, S.A.; Levine, J.E.; Laetsch, T.W.; Pulsipher, M.A.; Boyer, M.W.; August, K.J.; Hamilton, J.; Awasthi, R.; others. Clinical pharmacology of tisagenlecleucel in B-cell acute lymphoblastic leukemia. *Clinical Cancer Research* **2018**, *24*, 6175–6184.
24. Stein, A.M.; Grupp, S.A.; Levine, J.E.; Laetsch, T.W.; Pulsipher, M.A.; Boyer, M.W.; August, K.J.; Levine, B.L.; Tomassian, L.; Shah, S.; others. Tisagenlecleucel Model-Based Cellular Kinetic Analysis of Chimeric Antigen Receptor–T Cells. *CPT: pharmacometrics & systems pharmacology* **2019**, *8*, 285–295.
25. Chaudhury, A.; Zhu, X.; Chu, L.; Goliaei, A.; June, C.H.; Kearns, J.D.; Stein, A.M. Chimeric Antigen Receptor T Cell Therapies: A Review of Cellular Kinetic-Pharmacodynamic Modeling Approaches. *The Journal of Clinical Pharmacology* **2020**, *60*, S147–S159.
26. Sahoo, P.; Yang, X.; Abler, D.; Maestrini, D.; Adhikarla, V.; Frankhouser, D.; Cho, H.; Machuca, V.; Wang, D.; Barish, M.; others. Mathematical deconvolution of CAR T-cell proliferation and exhaustion from real-time killing assay data. *Journal of the Royal Society Interface* **2020**, *17*, 20190734.

27. León-Triana, O.; Pérez-Martínez, A.; Ramírez-Orellana, M.; Pérez-García, V.M. Dual-target CAR-Ts with on-and off-tumour activity may override immune suppression in solid cancers: A mathematical proof of concept. *Cancers* **2021**, *13*, 703.

28. Barros, L.R.C.; de Jesus Rodrigues, B.; Almeida, R.C. CAR-T cell Goes on a Mathematical Model. *Journal of Cellular Immunology* **2020**, *2*, 31–37.

29. Khatun, M.S.; Biswas, M.H.A. Modeling the effect of adoptive T cell therapy for the treatment of leukemia. *Computational and Mathematical Methods* **2020**, *2*, e1069.

30. Owens, K.; Bozic, I. Modeling CAR T-Cell Therapy with Patient Preconditioning. *Bulletin of Mathematical Biology* **2021**, *83*, 1–36.

31. Barros, L.R.C.; Paixão, E.A.; Valli, A.M.P.; Naozuka, G.T.; Fassoni, A.C.; Almeida, R.C.C. CARTmath-A Mathematical Model of CAR-T Immunotherapy in Preclinical Models. *Preprints* **2021**.

32. Kimmel, G.J.; Locke, F.L.; Altrock, P.M. The roles of T cell competition and stochastic extinction events in chimeric antigen receptor T cell therapy. *Proceedings of the Royal Society B* **2021**, *288*, 20210229.

33. Hardiansyah, D.; Ng, C.M. Quantitative Systems Pharmacology Model of Chimeric Antigen Receptor T-Cell Therapy. *Clinical and Translational Science* **2019**, *12*, 343–349.

34. Pérez-García, V.M.; León-Triana, O.; Rosa, M.; Pérez-Martínez, A. CAR T cells for T-cell leukemias: Insights from mathematical models. *Communications in Nonlinear Science and Numerical Simulation* **2021**, *96*, 105684.

35. Mostolizadeh, R.; Afsharnezhad, Z.; Marciniak-Czochra, A. Mathematical model of chimeric anti-gene receptor (CAR) T cell therapy with presence of cytokine. *Numerical Algebra, Control & Optimization* **2018**, *8*, 63.

36. León-Triana, O.; Sabir, S.; Calvo, G.F.; Belmonte-Beitia, J.; Chulián, S.; Álvaro Martínez-Rubio.; Rosa, M.; Pérez-Martínez, A.; Ramirez-Orellana, M.; Pérez-García, V.M. CAR T cell therapy in B-cell acute lymphoblastic leukaemia: Insights from mathematical models. *Communications in Nonlinear Science and Numerical Simulation* **2021**, *94*, 105570.

37. Murphy, K.; Weaver, C. *Janeway's Immunobiology*; Garland science, 2016.

38. Lucio, P.; Parreira, A.; Van den Beemd, M.; Van Lochem, E.; Van Wering, E.; Baars, E.; Porwit-MacDonald, A.; Bjorklund, E.; Gaipa, G.; Biondi, A.; others. Flow cytometric analysis of normal B cell differentiation: a frame of reference for the detection of minimal residual disease in precursor-B-ALL. *Leukemia* **1999**, *13*, 419–427.

39. Bevan, M.J. Helping the CD8+ T-cell response. *Nature Reviews Immunology* **2004**, *4*, 595–602.

40. Chulián, S.; Álvaro Martínez-Rubio.; Marciniak-Czochra, A.; Stiehl, T.; Goñi, C.B.; Rodríguez Gutiérrez, J.F.; Orellana, M.R.; Robleda, A.C.; Pérez-García, V.M.; Rosa, M. Dynamical properties of feedback signalling in B lymphopoiesis: A mathematical modelling approach. *Journal of Theoretical Biology* **2021**, 110685.

41. Chulián, S.; Rubio, Á.M.; Rosa, M.; Pérez-García, V.M. Mathematical models of Leukaemia and its treatment: A review. *arXiv preprint arXiv:2011.05881* **2020**.

42. Terwilliger, T.; Abdul-Hay, M. Acute lymphoblastic leukemia: a comprehensive review and 2017 update. *Blood Cancer Journal* **2017**, *7*, e577–e577.

43. De Boer, R.J.; Perelson, A.S. Quantifying T lymphocyte turnover. *Journal of Theoretical Biology* **2013**, *327*, 45–87.

44. Kaech, S.M.; Wherry, E.J.; Ahmed, R. Effector and memory T-cell differentiation: implications for vaccine development. *Nature Reviews Immunology* **2002**, *2*, 251–262.

45. Ahmed, R.; Bevan, M.J.; Reiner, S.L.; Fearon, D.T. The precursors of memory: models and controversies. *Nature Reviews Immunology* **2009**, *9*, 662–668.

46. De Boer, R.J.; Oprea, M.; Antia, R.; Murali-Krishna, K.; Ahmed, R.; Perelson, A.S. Recruitment times, proliferation, and apoptosis rates during the CD8+ T-cell response to lymphocytic choriomeningitis virus. *Journal of Virology* **2001**, *75*, 10663–10669.

47. De Boer, R.J.; Perelson, A.S. Towards a general function describing T cell proliferation. *Journal of Theoretical Biology* **1995**, *175*, 567–576.

48. Grossman, Z.; Min, B.; Meier-Schellersheim, M.; Paul, W.E. Concomitant regulation of T-cell activation and homeostasis. *Nature Reviews Immunology* **2004**, *4*, 387–395.

49. Ganusov, V.V.; Barber, D.L.; De Boer, R.J. Killing of targets by CD8+ T cells in the mouse spleen follows the law of mass action. *PLOS One* **2011**, *6*, e15959.

50. Passegué, E.; Wagers, A.J.; Giuriato, S.; Anderson, W.C.; Weissman, I.L. Global analysis of proliferation and cell cycle gene expression in the regulation of hematopoietic stem and progenitor cell fates. *The Journal of Experimental Medicine* **2005**, *202*, 1599–1611.

51. Pelayo, R.; Miyazaki, K.; Huang, J.; Garrett, K.P.; Osmond, D.G.; Kincade, P.W. Cell cycle quiescence of early lymphoid progenitors in adult bone marrow. *Stem Cells* **2006**, *24*, 2703–2713.

52. Matarraz, S.; Lopez, A.; Barrena, S.; Fernández, C.; Jensen, E.; Flores, J.; Bárcena, P.; Rasillo, A.; Sayagués, J.M.; Sánchez, M.; others. The immunophenotype of different immature, myeloid and B-cell lineage-committed CD34+ hematopoietic cells allows discrimination between normal/reactive and myelodysplastic syndrome precursors. *Leukemia* **2008**, *22*, 1175–1183.

53. Nombela-Arrieta, C.; Manz, M.G. Quantification and three-dimensional microanatomical organization of the bone marrow. *Blood Advances* **2017**, *1*, 407–416.

54. Ademokun, A.A.; Dunn-Walters, D. Immune responses: primary and secondary. *eLS* **2010**.

55. Kaech, S.M.; Ahmed, R. Memory CD8+ T cell differentiation: initial antigen encounter triggers a developmental program in naive cells. *Nature Immunology* **2001**, *2*, 415–422.

56. Wong, P.; Pamer, E.G. Cutting edge: antigen-independent CD8 T cell proliferation. *The Journal of Immunology* **2001**, *166*, 5864–5868.

57. Fraietta, J.A.; Nobles, C.L.; Sammons, M.A.; Lundh, S.; Carty, S.A.; Reich, T.J.; Cogdill, A.P.; Morrissette, J.J.; DeNizio, J.E.; Reddy, S.; others. Disruption of TET2 promotes the therapeutic efficacy of CD19-targeted T cells. *Nature* **2018**, *558*, 307–312.

58. Mikhailova, E.; Semchenkova, A.; Illarionova, O.; Kashpor, S.; Brilliantova, V.; Zakharova, E.; Zerkalenkova, E.; Zangrando, A.; Bocharova, N.; Shelikhova, L.; others. Relative expansion of CD19-negative very-early normal B-cell precursors in children with acute lymphoblastic leukaemia after CD19 targeting by blinatumomab and CAR-T cell therapy: implications for flow cytometric detection of minimal residual disease. *British Journal of Haematology* **2021**.

59. Awasthi, R.; Mueller, K.T.; Yanik, G.A.; Tam, C.S.; Rives, S.; McGuirk, J.P.; Pulsipher, M.A.; Boyer, M.W.; Jaeger, U.; Baruchel, A.; others. Evaluation of in vivo CAR transgene levels in relapsed/refractory pediatric and young adult ALL and adult DLBCL tisagenlecleucel-treated patients. *Blood* **2018**, *132*, 899–899.

60. Wudhikarn, K.; Park, J.H. Dissecting factors influencing response to CAR T cell therapy in B lymphoid hematologic malignancies: from basic to practice. *Leukemia & Lymphoma* **2020**, *61*, 1–11.

61. Awasthi, R.; Mueller, K.T.; Yanik, G.A.; Tam, C.S.L.; Rives, S.; McGuirk, J.; Boyer, M.W.; Jäger, U.; Baruchel, A.; Myers, G.D.; Borchmann, P.; Jaglowski, S.M.; Stefanski, H.E.; Bishop, M.R.; Waldron, E.K.; Hamilton, J.; Cota, M.; Bubuteishvili-Pacaud, L.; Waller, E.K. Considerations for tisagenlecleucel dosing rationale. *Journal of Clinical Oncology* **2018**, *36*, e15056–e15056.

62. Finney, O.C.; Brakke, H.; Rawlings-Rhea, S.; Hicks, R.; Doolittle, D.; Lopez, M.; Futrell, B.; Orentas, R.J.; Li, D.; Gardner, R.; others. CD19 CAR T cell product and disease attributes predict leukemia remission durability. *Journal of Clinical Investigation* **2019**, *129*, 2123–2132.

63. Chmielewski, M.; Abken, H. TRUCKs: the fourth generation of CARs. *Expert Opinion on Biological Therapy* **2015**, *15*, 1145–1154.

64. Singh, N.; Lee, Y.G.; Shestova, O.; Ravikumar, P.; Hayer, K.E.; Hong, S.J.; Lu, X.M.; Pajarillo, R.; Agarwal, S.; Kuramitsu, S.; others. Impaired death receptor signaling in leukemia causes antigen-independent resistance by inducing CAR T-cell dysfunction. *Cancer Discovery* **2020**, *10*, 552–567.

65. Feucht, J.; Sun, J.; Eyquem, J.; Ho, Y.J.; Zhao, Z.; Leibold, J.; Dobrin, A.; Cabriolu, A.; Hamieh, M.; Sadelain, M. Calibration of CAR activation potential directs alternative T cell fates and therapeutic potency. *Nature Medicine* **2019**, *25*, 82–88.

66. Ghorashian, S.; Kramer, A.M.; Onuoha, S.; Wright, G.; Bartram, J.; Richardson, R.; Albon, S.J.; Casanovas-Company, J.; Castro, F.; Popova, B.; others. Enhanced CAR T cell expansion and prolonged persistence in pediatric patients with ALL treated with a low-affinity CD19 CAR. *Nature Medicine* **2019**, *25*, 1408–1414.

67. Turtle, C.J.; Hanafi, L.A.; Berger, C.; Gooley, T.A.; Cherian, S.; Hudecek, M.; Sommermeyer, D.; Melville, K.; Pender, B.; Budiarto, T.M.; others. CD19 CAR–T cells of defined CD4+: CD8+ composition in adult B cell ALL patients. *Journal of clinical investigation* **2016**, *126*, 2123–2138.

68. Gauthier, J.; Bezerra, E.D.; Hirayama, A.V.; Fiorenza, S.; Sheih, A.; Chou, C.K.; Kimble, E.L.; Pender, B.S.; Hawkins, R.M.; Vakil, A.; others. Factors associated with outcomes after a second CD19-targeted CAR T-cell infusion for refractory B-cell malignancies. *Blood* **2021**, *137*, 323–335.

69. Nie, Y.; Lu, W.; Chen, D.; Tu, H.; Guo, Z.; Zhou, X.; Li, M.; Tu, S.; Li, Y. Mechanisms underlying CD19-positive ALL relapse after anti-CD19 CAR T cell therapy and associated strategies. *Biomarker Research* **2020**, *8*, 1–17.

70. Annesley, C.; Gardner, R.; Wilson, A.; Summers, C.; Lamble, A.J.; Rivers, J.; Wu, Q.V.; Brand, A.; Johnson, A.; Spratt, K.; Mgebroff, S.; Brown, C.; Lindgren, C.; Park, J.R.; Jensen, M.C. Novel CD19t T-Antigen Presenting Cells Expand CD19 CAR T Cells In Vivo. *Blood* **2019**, *134*, 223–223.

71. Ma, F.; Ho, J.Y.; Du, H.; Xuan, F.; Wu, X.; Wang, Q.; Wang, L.; Liu, Y.; Ba, M.; Wang, Y.; others. Evidence of long-lasting anti-CD19 activity of engrafted CD19 chimeric antigen receptor–modified T cells in a phase I study targeting pediatrics with acute lymphoblastic leukemia. *Hematological Oncology* **2019**, *37*, 601–608.

72. Wherry, E.J. T cell exhaustion. *Nature Immunology* **2011**, *12*, 492–499.

73. Mueller, S.N.; Ahmed, R. High antigen levels are the cause of T cell exhaustion during chronic viral infection. *Proceedings of the National Academy of Sciences* **2009**, *106*, 8623–8628.